arXiv:1602.03335v2 [cond-mat.str-el] 29 Jun 2016

Spin wave excitations in the tetragonal double perovskite Sr_2CuWO_6

H. C. Walker,[1] O. Mustonen,[2] S. Vasala,[2,3] D. J. Voneshen,[1] M. D. Le,[1] D. T. Adroja,[1,4] and M. Karppinen[2]

[1] *ISIS Neutron and Muon Source, Rutherford Appleton Laboratory, Chilton, Didcot, OX11 0QX, United Kingdom*
[2] *Department of Chemistry, Aalto University, FI-00076 Aalto, Finland*
[3] *Laboratory of Photonics and Interfaces, École Polytechnique Fédérale de Lausanne, CH-1015 Lausanne, Switzerland*
[4] *Highly Correlated Matter Research Group, Physics Department, University of Johannesburg, P.O. Box 524, Auckland Park 2006, South Africa*

(Dated: June 30, 2016)

Sr_2CuWO_6 is a double perovskite proposed to be at the border between two and three dimensional magnetism, with a square lattice of $S = \frac{1}{2}$ Cu^{2+} ions. We have used inelastic neutron scattering to investigate the spin wave excitations of the system, to find out how they evolve as a function of temperature, as well as to obtain information about the magnetic exchange interactions. We observed well defined dispersive spin wave modes at 6 K, which partially survive above the magnetic ordering temperature, $T_N = 24$ K. Linear spin wave theory is used to determine the exchange interactions revealing them to be highly two-dimensional in nature. Density functional theory calculations are presented supporting this experimental finding, which is in contrast to a previous *ab-initio* study of the magnetic interactions. Our analysis confirms that not the nearest neighbour, but the next nearest neighbour interactions in the tetragonal *ab* plane are the strongest. Low incident energy measurements reveal the opening of a 0.6(1) meV gap below T_N, which suggests the presence of a very weak single ion anisotropy term in the form of an easy axis along $\hat{\mathbf{a}}$.

PACS numbers: 78.70.Nx, 75.30.Ds, 75.50.Ee

I. INTRODUCTION

Low dimensional magnetism is currently of great interest to condensed matter physics, partly due to the link to the two dimensional antiferromagnetic parent phases of the high-T_c superconductors[1,2]. In those compounds it is considered that the square lattice of $S = \frac{1}{2}$ Cu^{2+} $3d^9$ ions is responsible for their magnetic and superconducting behaviour. They possess strong in-plane nearest neighbour (NN) superexchange ($J \sim 130$ meV) and weaker next nearest (NNN) exchange ($J' \sim 18$ meV)[3–5]. Similar copper square lattice compounds with weaker interactions are of interest as a point of comparison for the fundamental understanding of the magnetism of square lattices of Cu^{2+} ions.

The *B*-site ordered double perovskite oxides $Sr_2CuB''O_6$, where B'' is a diamagnetic hexavalent ion such as Mo, Te or W, are examples of such materials[6]. Although they are structurally three dimensional, many display low dimensional properties. The *ab* planes have a square centred array of Cu^{2+}, with the half-filled Cu $3d_{x^2-y^2}$ orbitals ordered into the *ab* planes by the Jahn-Teller distortion, creating magnetic interactions between the neighbouring Cu ions within the *ab* planes. As the d_{z^2}, d_{yz} and d_{zx} orbitals are all filled, the magnetic interactions along the *c* axis are expected to be weak, resulting in the magnetic interactions being quasi two-dimensional[7]. Compared to the interactions in the cuprates, in the double perovskites the magnetic ions are separated by an array of diamagnetic O-B''-O ions, making them an order of magnitude weaker, and therefore it is possible to study the low temperature low dimensional magnetic properties.

Sr_2CuWO_6 shows a broad maximum in the magnetic susceptibility at 83 K, behaviour characteristic of two-dimensional Quantum Square Lattice Heisenberg Antiferromagnets (QSLHAF), with no clear indication of a transition to a long-range-ordered magnetic state[8]. There is a kink in the second derivative at 24 K, but the data are inconclusive of any transition. Instead the transition to a long-ranged ordered state was confirmed definitively via μSR, with the observation of a spontaneous oscillation below 24 K, and only a slowly decaying component above, with no sign of quasistatic short-range order[8]. Regrettably there was insufficient data for the

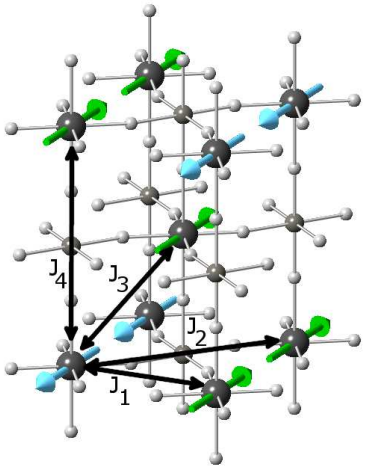

FIG. 1. Schematic view of the magnetic structure and exchange constants J_1 to J_4 between Cu ions in double perovskite Sr_2CuWO_6. Large dark spheres are Cu, smaller spheres are W and the smallest palest spheres are O. Sr has been omitted for clarity.

temperature dependence of the local magnetic field to determine unambiguously whether the ordering is $3D$ or lower dimensional.

High flux neutron powder diffraction data have revealed that the Cu^{2+} ions display antiferromagnetic Type-II ordering with $0.57(1)\mu_B$ magnetic moments aligned along the a-axis[9], see Figure 1. The moment is smaller than might be expected for $S = \frac{1}{2}$ Cu^{2+} ions ($m_s = g \times j = g \times s = 1\mu_B$), possibly due to a degree of frustration or being on the borderline between quasi-low dimensional and three dimensional magnetism. It may also be the signature of quantum zero-point fluctuations, which can reduce the moment in QSLHAF systems[10].

Electronic structure calculations, using a Coulomb U value determined in relation to oxygen K-edge X-ray absorption spectroscopy measurements, gave the exchange constants: $J_1 = -1.20$, $J_2 = -7.47$, $J_3 = -0.03$ and $J_4 = -4.21$ meV, resulting in a reasonable agreement with the measured Curie-Weiss temperature ($\theta_{\rm meas} = -116$ K, $\theta_{\rm calc} = -126$ K)[8]. These values are consistent with the observed Type II antiferromagnetic structure[9], but the interplanar J_4 coupling indicates significantly stronger three dimensional magnetism than might have been expected from the electronic structure and based on the form of the magnetic susceptibility. To investigate this apparent discrepancy we have performed inelastic neutron scattering (INS) measurements and a comprehensive Density Functional Theory (DFT) study to re-examine the exchange constants in Sr_2CuWO_6.

In this paper we present our inelastic neutron scattering measurements performed on Sr_2CuWO_6. The INS results are analysed and compared with linear spin wave theory simulations based on the original DFT estimates[8] for the exchange interactions. This demonstrates a significant disagreement with the earlier DFT calculations. We have reassessed the DFT calculations and present revised results, which support the conclusions drawn from our INS data indicating a strong two dimensional character, and revealing the significance of the straight Cu-O-W-O-Cu linkers.

II. EXPERIMENTAL DETAILS

A 6.89 g powder sample of $Sr_2CuWO_6$was synthesized by solid-state reaction of a stoichiometric mixture of $SrCO_3$, CuO and WO_3 powders, according to the method detailed in Ref. 8. The phase purity and quality of the sample were verified using x-ray diffraction (X'Pert Pro MPD, Cu K_{α_1} radiation). Rietveld refinement using the FULLPROF program[11] confirmed that the sample is single phase with the $I4/m$ structure and lattice parameters $a = 5.430(2)$ Å and $c = 8.415(2)$ Å as reported earlier[8].

Neutron inelastic scattering measurements were performed on the MERLIN time-of-flight direct geometry spectrometer[12] at the ISIS facility of the Rutherford Appleton Laboratory. The sample was contained in an aluminium foil packet in the form of an annulus of diameter 40 mm and height 40 mm and sealed in a thin aluminium can containing helium exchange gas. The sample can was cooled by a closed-cycle refrigerator. The straight Gd slit package was used in the Fermi chopper, which was phased to allow the recording of spectra with incident energies of either 18 and 45 meV (at a rotation speed of 250 Hz), or 10 and 34 meV (at a rotations speed of 150 Hz) simultaneously via the rep-rate multiplication method[13–15]. The data were collected at a series of temperatures between $T = 6$ and 93 K for ~ 4 h each. The data were reduced using the MantidPlot software package[16]. The raw data were corrected for detector efficiency and time independent background following standard procedures[17]. Vanadium spectra were recorded[18] with the same incident energies to determine the energy resolution and to convert the intensities into units of cross section, mb.sr^{-1}.meV^{-1}.f.u.$^{-1}$, where f.u. stands for the formula unit of Sr_2CuWO_6. Additional measurements with $E_i = 1.9, 3.5, 8.3$ meV at a chopper frequency of 100 Hz were performed on the same sample on the LET time-of-flight direct geometry spectrometer[19] also using the rep-rate multiplication method.

III. COMPUTATIONAL DETAILS

The exchange constants $J_1 - J_4$ can be obtained using DFT by calculating the energy differences between multiple collinear spin states and projecting those onto the following Hamiltonian:

$$H = -\sum_{ij} J_{ij} \mathbf{S}_i \cdot \mathbf{S}_j, \tag{1}$$

This is known as the mapping method.[20,21] One ferromagnetic and four antiferromagnetic collinear spin states are sufficient in Sr_2CuWO_6, see ref.8 for more details. These configurations are presented in Figure 2 and consist of $2\times2\times1$ (AFM1-3) or $1\times1\times2$ (AFM4) supercells. The exchange constants can be solved from the following equations:

$$J_3 = \left(E_{\rm AFM1} - E_{\rm FM}\right)/16S^2, \tag{2}$$

$$J_1 = \left(E_{\rm AFM2} - E_{\rm FM} - 8J_3S^2\right)/8S^2, \tag{3}$$

$$J_2 = \left(E_{\rm AFM3} - E_{\rm FM} - 4J_1S^2 - 8J_3S^2\right)/8S^2, \tag{4}$$

$$J_4 = \left(E_{\rm AFM4} - E_{\rm FM} - 8J_3S^2\right)/4S^2. \tag{5}$$

Total energies of the spin configurations were determined by means of density functional theory calculations using the full-potential linearised augmented plane-wave plus local orbitals (FP-LAPW+lo) ELK code[22]. The calculations were performed using the experimental crystal structure of Sr_2CuWO_6 determined by neutron diffraction[8]. The generalised gradient approximation (GGA) exchange and correlation functionals by

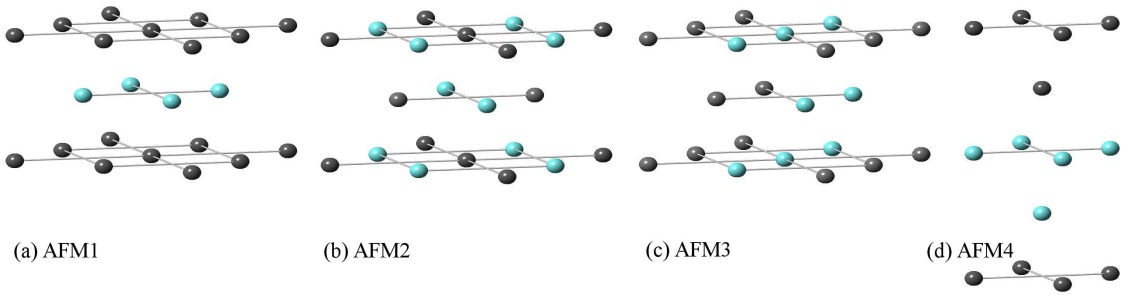

FIG. 2. Schematic of the four AFM orderings used in calculating the magnetic exchange constants of Sr_2CuWO_6. Black and cyan spheres correspond to the two spin states on the Cu ions. Other ions and long bonds along the c-axis are omitted for clarity.

Perdew, Burke and Ernzerhof were used[23]. A k point mesh of either $4 \times 4 \times 6$ or $8 \times 8 \times 3$ was used depending on the supercell. The plane-wave cutoff was set at $|G+k|_{\mathbf{max}} = 8/R_{MT}$ a.u.$^{-1}$, where R_{MT} is the radius of the smallest muffin-tin (oxygen, 1.55 a.u.).

Sr_2CuWO_6 is a strongly correlated material, and thus electron correlation effects are central for modelling the electronic structure. The correlation effects of localised Cu^{2+} $3d$ electrons were included within the semi-empirical DFT+U framework with Hubbard U and Stoner I as parameters[24]. DFT+U methods such as GGA+U require the use of a double counting correction, since Coulomb and intra-atomic exchange interactions are also included in the GGA functionals. We have used both Around Mean Field (AMF)[25] and Fully Localised Limit (FLL)[26] double counting corrections in this work. Exchange constants calculated by DFT are known to be sensitive to the on-site Coulomb term U and the double counting correction used[27]. For this reason, we have calculated the exchange constants using a range of U values typical for Cu $3d$ with two different double counting corrections. With the FLL correction a Hubbard U of $\sim 8-9$ eV has been widely used for Cu in oxides,[24,26–28] whereas a slightly lower U of $\sim 6-7$ eV is typical when using the AMF correction[25,27]. The intra-atomic exchange parameter I was chosen to be 0.9 eV, which is a common value in $3d$ transition metal oxides[24].

In order to evaluate the overall strength of the exchange interactions with different Hubbard U values, we have calculated the Weiss temperature θ using the mean field approximation:

$$\theta = \frac{S(S+1)}{3k_B} \sum_i z_i J_i, \qquad (6)$$

where k_B is the Boltzmann constant and z_i is the number of sites connected by exchange interaction J_i.

IV. EXPERIMENTAL RESULTS

For temperatures below T_N, additional peaks are observed at the elastic line at $|Q| = 0.69$ Å and 1.35 Å, corresponding to the $(0\ \frac{1}{2}\ \frac{1}{2})$ and $(1\ \frac{1}{2}\ \frac{1}{2})$ magnetic Bragg peaks, confirming the previous assignment of Type II antiferromagnetic ordering described by a $[0\ \frac{1}{2}\ \frac{1}{2}]$ magnetic ordering wavevector[9]. The colour-coded inelastic neutron scattering intensity maps of Sr_2CuWO_6 measured on MERLIN at various temperatures between $T = 6$ and 93 K are shown in Figure 3(a-f). At low temperatures, for momentum transfer $|Q| < 4$ Å^{-1}, a strong flat scattering band can be observed at ~ 18 meV (Fig. 3). In addition steep spin waves are seen apparently emanating from the

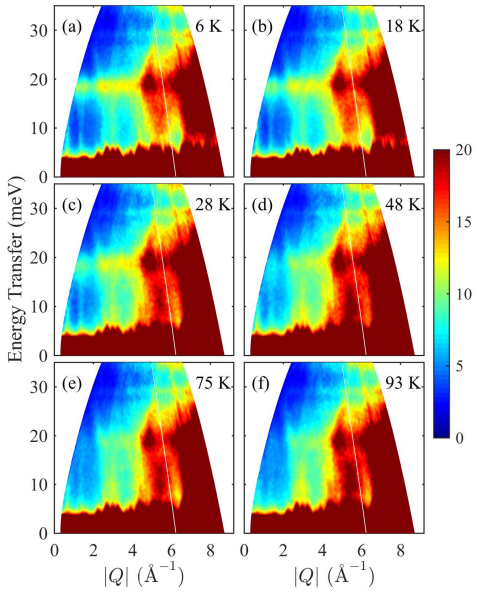

FIG. 3. (Colour online) Colour coded inelastic neutron scattering intensity maps in units of mb.sr^{-1}.meV^{-1}.f.u.$^{-1}$, energy transfer vs momentum transfer Q of Sr_2CuWO_6 measured with an incident energy of $E_i = 45$ meV on MERLIN.

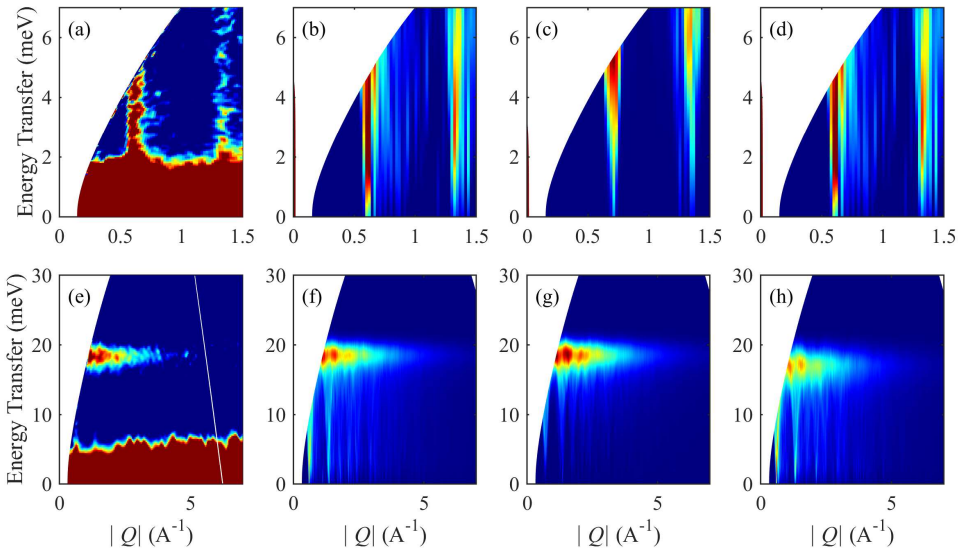

FIG. 4. (Colour online) The measured magnetic scattering at 6 K after phonon scattering subtraction for (a) $E_i = 10$ and (e) $E_i = 45$ meV; compared with the spin wave scattering at 6 K simulated using the SpinW program with exchange parameters (b) and (f) optimised for the experimental data: $J_1 = -1.2$ meV, $J_2 = -9.5$ meV, $J_3 = 0$ meV and $J_4 = -0.01$ meV, (c) and (g) from a previous DFT study[8]: $J_1 = -1.20$ meV, $J_2 = -7.47$ meV, $J_3 = -0.03$ meV and $J_4 = -4.21$ meV, and (d) and (h) from the DFT study presented in Section V: $J_1 = -2.45$ meV, $J_2 = -8.83$ meV, $J_3 = 0$ meV and $J_4 = -0.01$ meV.

elastic line. Based on the measurements performed with an incident energy of 10 meV on MERLIN, these excitations would appear to be gapless to within the resolution of the instrument (FWHM$= 0.65 \pm 0.01$ meV). At larger $|Q|$ values the excitations are dominated by phonons.

Looking at the temperature evolution, the flat band at $\sim$ 18 meV appears to be more strongly effected by increasing temperature, disappearing between 28 K and 48 K, while evidence of the spin waves persists up to at least 75 K, i.e. well above $T_N = 24$ K, which indicates the presence of two dimensional interactions. These features are both absent at 93 K, above the broad maximum seen in the magnetic susceptibility at $T_{\max} = 83$ K[8]. The assignment of the higher $|Q|$ features as phonons is further confirmed by their increasing intensity with increasing temperature. By considering the Bose factor, and using the 93 K data we can subtract the phonons from the low temperature data to give the purely magnetic signal[29], as shown in Fig. 4(a) and (e).

In order to model the observed magnetic spectrum, we have calculated the spin wave dispersions, the spin-spin correlation function and the neutron scattering cross section using the SpinW program[30]. Since tungsten is hexavalent in Sr_2CuWO_6, it is diamagnetic, and therefore only interactions between the Cu^{2+} ions need to be considered. We have constructed the magnetic Hamiltonian in Eq. (1) with four different exchange couplings for the nearest and next nearest neighbour interactions in plane, and interplanar along the c-axis, as shown in Fig. 1. As we could not confirm the existence of a small spin gap to within the instrumental resolution of MERLIN, we initially neglect a single ion anisotropy term, which would generally open such a gap. For the spin wave calculation we started from the original DFT-calculated values of the exchange parameters given in Section I. Further the instrument resolution was estimated from vanadium runs and this was included in the simulation.

Comparing the simulation for the original DFT-determined exchange parameters[8] (Figs. 4(c) & (g)) with the measured spin wave dispersion (Figs. 4(a) & (e)) we see that the simulation accurately reproduces the band maximum at 18 meV, with steep spin waves emerging from the elastic line. However, closer inspection of the data reveals that the spin waves do not actually emerge from the magnetic Bragg peaks. Instead the centre of the lower $|Q|$ excitation is at 0.62 Å^{-1}, lying between 0.58 Å^{-1}, corresponding to the forbidden $(\frac{1}{2}00)$ position, and 0.69 Å^{-1}, corresponding to the allowed $(\frac{1}{2}0\frac{1}{2})$ position. In order to better reproduce the data, we have found a new set of exchange parameters: $J_1 = -1.2$ meV, $J_2 = -9.5$ meV, $J_3 = 0$ meV and $J_4 = -0.01$ meV, which are noticeably more two dimensional than those obtained originally using DFT[8], see the simulation panels Fig. 4(b) and (f). The difference in the two simulations can be seen more strikingly in Figure 5. While both manage to reproduce the band maximum at $\sim$ 18 meV (Fig. 5(a)), which is shown to follow the magnetic form factor for Cu^{2+} in Fig. 5(b); the cut through the excitations integrated for $4 < E < 6$ meV (Fig. 5(c)), shows how the original DFT-determined exchange parameters simulation inaccurately estimates the $|Q|$ position of the first excitation as emerging from the $(0\ \frac{1}{2}\ \frac{1}{2})$ magnetic

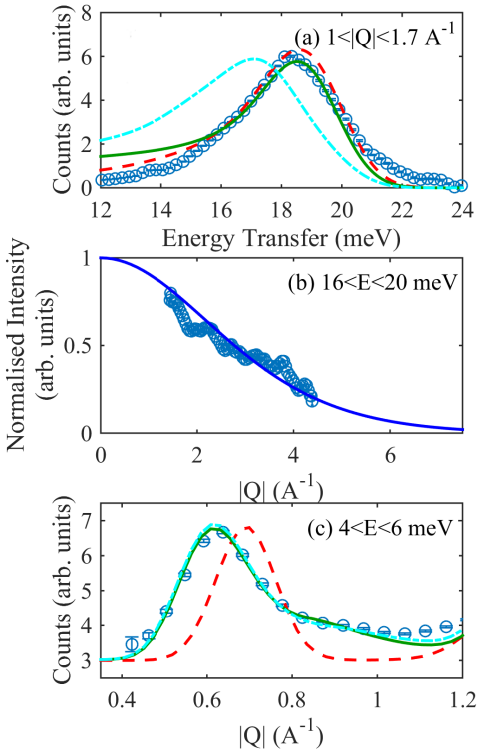

FIG. 5. (Colour online) One dimensional cuts of the magnetic scattering from Sr_2CuWO_6 at 6 K (a) intergrated between $1 < |Q| < 1.7$ Å^{-1} compared with the simulated powder average spin waves for the original DFT-determined exchange parameters (dashed red line) and for the more two dimensional INS obtained exchange parameters (solid green line), and for the best revised DFT exchange parameters (dot-dash cyan line), (b) a q-cut through the ~ 18 meV feature, showing that it follows the magnetic form factor for Cu^{2+}, and (c) a q-cut through the data integrated between $4 < E < 6$ meV compared with simulations for the original DFT-determined exchange parameters (dashed red line), for the more two dimensional INS obtained exchange parameters (solid green line) and for the best revised DFT exchange parameters (dot-dash cyan line).

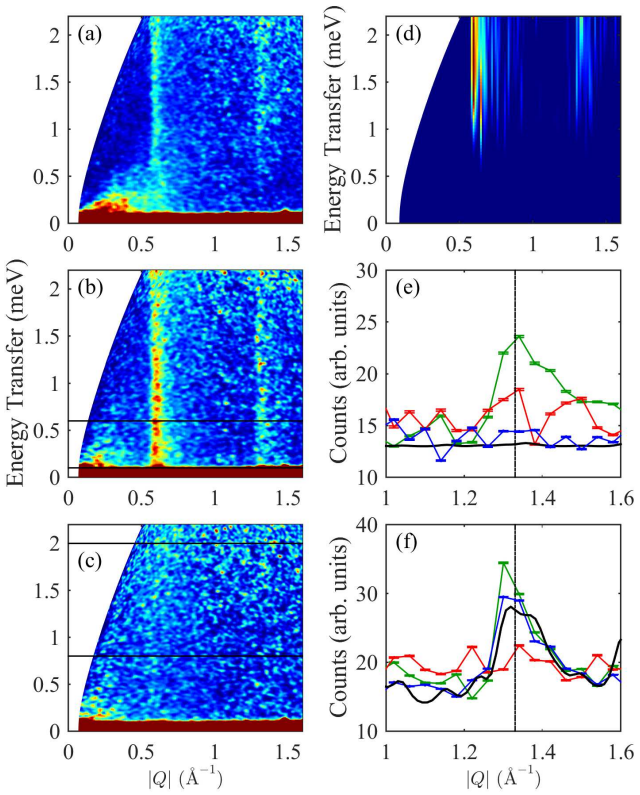

FIG. 6. (Colour online) The magnetic scattering data for $E_i = 3.51$ meV at (a) 5 K, (b) 30 K and (c) 100 K. (d) shows a SpinW simulation for the low temperature data, reproducing a gap with the addition of single ion anisotropy term. One dimensional cuts through the data at 5 K (blue), 30 K (green) and 100 K (red) for (e) $0.1 < E < 0.6$ meV and (f) $0.8 < E < 2$ meV are compared with cuts through the simulation (black line).

Bragg peak, while the simulation for the new exchange parameters reproduces the data well. When the simulation for the new experimental exchange parameters is performed to obtain the single crystal dispersion, it becomes clear that the excitations are emerging from both the $(\frac{1}{2}0\frac{1}{2})$ and $(\frac{1}{2}00)$ positions, and it is the powder averaging that gives rise to the observed 0.62 Å^{-1} position. In order to understand the appearance of the softening at the forbidden $(\frac{1}{2}00)$ position, it is necessary to look at the value of J_4. If J_4 were ferromagnetic, then Type I antiferromagnetic order would be stabilised. Our value for J_4 of only -10μeV puts Sr_2CuWO_6 close to the border between Type I and Type II ordering, such that softening is observed at both positions, but the negative sign results in Type II order.

In optimising our exchange parameters to fit the data, it is made clear that the value of J_2 is central to the position of the band maximum. Simulations for the spin wave dispersion indicate that the value of J_1 modulates the spin wave maxima over different positions in the Brillouin Zone, that on powder averaging leads to a broadening of the 18 meV band maximum. We have estimated J_1 based on the width of the peak in Fig. 5(a), taking the instrumental resolution at an energy transfer of 18 meV into account.

While the energy resolution on MERLIN did not allow us to observe a spin gap, by using the cold chopper spectrometer LET we are able to distinguish the presence of a small gap of order 0.6(1) meV below T_N. Figure 6 shows the temperature evolution of this gap. Below T_N (Fig. 6(a)) the gap is present, although somewhat obscured for the lower $|Q|$ excitation by the presence of a spurious signal close to the beam stop. When the temperature is raised above T_N the gap closes, with strong spectral weight shifted down to the elastic line (Fig. 6(b)). Fi-

TABLE I. Exchange constants of Sr_2CuWO_6 calculated by GGA+U using the mapping method compared with the results obtained from inelastic neutron scattering.

	AMF				FLL			INS
U (eV)	5	6	7	8	7	8	9	-
J_1 (meV)	-3.70	-3.18	-2.70	-2.56	-3.29	-2.45	-2.58	-1.2
J_2 (meV)	-13.83	-10.87	-7.96	-6.23	-10.42	-8.83	-6.75	-9.5
J_3 (meV)	0.01	0.06	-0.06	-0.04	-0.02	0.03	-0.04	0
J_4 (meV)	0.12	0.03	0.19	0.07	0.09	0.04	-0.12	-0.01
J_2/J_1	3.73	3.42	2.95	3.61	3.16	3.61	2.61	7.92
θ (K)	-202.5	-161.4	-102.4	-102.4	-159.1	-129.9	-110.0	-124.1

nally, above $T_{\max}$, the excitations are entirely absent. We have been able to reproduce the presence of the gap in the ordered structure in our SpinW simulations (Fig. 6(d)) by modifying Eq. (1) to include single ion anisotropy in the form of an easy axis along $\hat{\mathbf{a}}$ of magnitude 0.025 meV. Although it is commonly believed that magnetic systems of spin-1/2 transition-metal ions have no magnetic anisotropy arising from spin-orbit coupling[31], this is only the case for ions in a perfect octahedral crystal field (t_{2g} ground state). Any distortion which splits the triply degenerate ground state and mixes the orbital d-states can, via the spin-orbit coupling, give non-zero single ion anisotropy[32]. In Fig. 6(e) a cut along $|Q|$ integrating between 0.1 and 0.6 meV shows how peaks are only observed in the data for $T_N < T < T_{\max}$, while in Fig. 6(f) a cut integrating energies between 0.8 and 2.0 meV shows peaks for both $T_N < T < T_{\max}$ and $T < T_N$, where the lowest temperature data is well matched by the simulation.

V. COMPUTATIONAL RESULTS

The exchange constants calculated by DFT are presented in Table I. In all cases the main interactions are the in-plane J_1 and J_2 interactions, which are antiferromagnetic. These results show that the next-nearest neighbor J_2 interaction in Sr_2CuWO_6 is stronger than the nearest neighbor J_1 interaction, which is consistent with the experimental Type II magnetic structure[9]. The strength of the exchange interactions decreases with increasing Hubbard U, which is clearly seen from the change in Weiss temperatures. This decrease is typical when the mapping method is used with DFT+U[20,21].

The exchange constants obtained by AMF and FLL double counting corrections are similar, with FLL producing stronger interactions for the same Hubbard U. The computational results are in fairly good, but not perfect, agreement with the experimental INS results. The DFT calculations presented here consistently overestimate the nearest-neighbour J_1 interaction, which results in a rather lower J_2/J_1 ratio (~ 3) than experimentally observed (~ 8). J_2, in contrast, is in good agreement with the experimental results. The inter-planar interactions J_3 and J_4 are very weak compared to J_1 and J_2 in all solutions, which is consistent with the experimental exchange constants obtained by INS. This shows that the magnetic interactions in Sr_2CuWO_6 are highly two-dimensional. However, the correct negative sign (i.e. antiferromagnetic interaction) for J_4 is only obtained with FLL correction and $U = 9$ eV. This solution also results in a Weiss temperature of 110 K, which is the closest to the experimental value of 116 K[8], but the low value of J_2 leads to a sizeable underestimate of the band maximum. If J_3 and J_4 are constrained to be small and negative, then the best match to the experimental data is obtained for the FLL double counting correction with $U = 8$ eV, see Fig. 4(d) and (h), although they do not exactly reproduce the inelastic neutron scattering data, underestimating the band maximum position and overestimating the width (Fig. 5(a)).

The previous DFT study of Sr_2CuWO_6[8] found a far stronger J_4 interaction of -4.21 meV, indicating significantly more three-dimensional magnetism than reported here. The difference between the results presented in Table I and those published previously[8] is perhaps due to the new calculations being performed over a range of U values with a more accurate crystal structure, higher plane-wave cut-off and a newer branch of the ELK code, although the exact origin of this discrepancy is not known.

VI. DISCUSSION

Now we compare the exchange parameters estimated for Sr_2CuWO_6 with those of Sr_2CuTeO_6[33,34]. Based on magnetic susceptibility measurements, it is estimated that in isostructural Sr_2CuTeO_6 the ratio $J_2/J_1 < 0.07$[33], compared to ~ 8 in Sr_2CuWO_6 from the INS results, while recent inelastic neutron scattering measurements have reduced the Sr_2CuTeO_6 value even further to 0.03[34]. Koga *et al.* propose that this reversal in relative strengths of nearest and next nearest neighbour interactions is due to the outermost filled orbital in Te^{6+} being $d_{x^2-y^2}$, such that the two hole spins must be antiparallel, giving antiferromagnetic exchange J_1 and J_2; whereas in W^{6+} the p_x and p_y orbitals are orthogonal so that the two hole spins are parallel, which would give a ferromagnetic exchange for J_1 and an antiferromagnetic exchange for J_2. However, our DFT calculations and spin wave analysis indicates a weak but antiferromagnetic J_1

in Sr_2CuWO_6, which might be due to the presence of frustration. Babkevich *et al.* have combined their INS measurements on Sr_2CuTeO_6 with *ab-initio* calculations, which have revealed that, in fact, the dominant exchange path is via Cu-O-O-Cu, and not via the Te $4d$ orbitals.

It is interesting to also compare the inelastic neutron scattering results from $3d$ double perovskite Sr_2CuWO_6 with those reported for $4d$ and $5d$ double perovskites with monoclinic, tetragonal or cubic crystal structures. It is to be noted that in the cubic (or less distorted monoclinic) structure of double perovskites with a single magnetic ion, the magnetic lattice is face centred cubic, which is a geometrically frustrated lattice and provides a unique opportunity to investigate frustrated magnetism. The inelastic neutron scattering study of face centred cubic Ba_2YMoO_6 (Mo^{5+} $4d^1$ $S = \frac{1}{2}$) demonstrates the existence and temperature dependence of a gapped magnetic excitation at 28 meV, with a bandwidth of 4 meV[29]. The observed dispersive triplet excitations come from a singlet ground state formed from orthogonal dimers on the Mo^{5+} tetrahedra. On the other hand, an inelastic neutron scattering study on monoclinic La_2NaRuO_6 also reveals a spin gap of 2.75 meV. As the magnetic anisotropy is expected to be small for octahedrally-coordinated Ru^{5+} $4d^3$ $S = \frac{3}{2}$ systems, the large gap observed for La_2NaRuO_6 may originate from the significantly enhanced value of the spin-orbit coupling in this $4d$ material[35]. FCC Ba_2YRuO_6 also displays a ~ 5 meV spin gap, with a zone boundary energy of 14 meV, at the [100] magnetic ordering wavevector below $T_N = 26$ K[36]. INS has also revealed well defined dispersive spin wave excitations in a polycrystalline sample of monoclinic Sr_2YRuO_6, with a zone boundary energy of ~ 8 meV at $T = 5$ K and a gap of 1.2 meV below 20 K, but gapless above, despite being well below $T_N = 31$ K[37]. The presence of strong diffusive scattering between T_N and 300 K is indicative of strong magnetic frustration between Ru-Ru atoms. The estimated exchange interactions give a ratio between nearest and next nearest neighbours $J_2/J_1 \sim 0.14$, revealing much stronger nearest neighbour interactions in contrast to $Sr_2CuWO_6(J_2/J_1 \sim 8)$.

Further instructive comparison might be made with other $S = 1/2$ Cu^{2+} quantum square lattice Heisenberg antiferromagnets (QSLHAF), which have been of considerable interest both theoretically and experimentally ever since the realisation that the parent compounds of the cuprate superconductors could be described using the same model. The low energy dynamics of QSLHAF are well described using linear spin wave theory with quantum corrections. However, inelastic neutron scattering measurements on a range of Cu^{2+} QSLHAF have revealed a glaring anomaly at high energy in the vicinity of $\mathbf{q} = (\pi, 0)$, where the intensity of the otherwise sharp excitations is completely wiped out[5,38–41]. Identifying the origin of this effect is complicated by the presence of additional exchange terms such as electronic ring exchange[5,38] and further neighbour exchange[39], as is also present in Sr_2CuWO_6. Due to similarities in the measured anomaly with predictions for fermionic Resonating Valence Bond excitations[42], it has been speculated that the anomaly may be related to fractionalised spin excitations[5,40]. By analogy with 1-D systems, these are referred to as spinons. In 1-D spinons have been identified in a number of materials, but observing 2-D analogues has proved more challenging until recently[41]. It would therefore clearly be very interesting to measure the excitations in single crystal Sr_2CuWO_6.

VII. CONCLUSIONS

We have performed inelastic neutron scattering measurements on double perovskite Sr_2CuWO_6, which reveal clear evidence of spin wave excitations at low temperatures. The magnetic excitations partially survive at temperatures above $T_N = 24$ K for long range 3D order, indicating a 2D component to the nature of the magnetic interaction. Our spin wave analysis using linear spin wave theory indicates that the NNN interaction in the ab plane is a factor of approximately eight times stronger compared to the NN interaction in the ab plane. While a previous DFT study gave a ratio of 1.78 for the strong interactions in plane (J_2) and interplane (J_4), our inelastic neutron scattering results indicate that J_2 is significantly stronger than J_4, which is consistent with the expected two dimensional behaviour given the Jahn-Teller distortion. The more comprehensive DFT study presented here has obtained results supporting this two dimensional nature and the dominance of the NNN interaction. The strongest interaction in the ab plane is most probably arising due to superexchange between the Cu^{2+} $d_{x^2-y^2}$ orbitals via the Oxygen p orbitals along straight linkers. Furthermore, the observation of a very small spin gap in Sr_2CuWO_6 is in line with a general explanation, which attributes the opening of increasingly large spin gaps in $4d$ and $5d$ systems as being due to the stronger spin orbit coupling compared to that in $3d$ systems.

Upon submission we were made aware of another paper reporting inelastic neutron scattering measurements on Sr_2CuWO_6[43].

ACKNOWLEDGMENTS

The authors acknowledge CSC-IT Centre for Science, Finland, for providing computational resources. DTA would like to thank JSPS for funding his visit to Hiroshima University.

[1] P. Dai, Rev Mod Phys **87**, 855 (2015).
[2] B. Keimer, S. A. Kivelson, M. R. Norman, S. Uchida, and J. Zaanen, Nature **518**, 179 (2015).
[3] S. M. Hayden, G. Aeppli, R. Osborn, A. D. Taylor, T. G. Perring, S.-W. Cheong, and Z. Fisk, Phys. Rev. Lett. **67**, 3622 (1991).
[4] R. Coldea, S. M. Hayden, G. Aeppli, T. G. Perring, C. D. Frost, T. E. Mason, S.-W. Cheong, and Z. Fisk, Phys. Rev. Lett. **86**, 5377 (2001).
[5] N. S. Headings, S. M. Hayden, R. Coldea, and T. G. Perring, Phys. Rev. Lett. **105**, 247001 (2010).
[6] S. Vasala and M. Karppinen, Progress in Solid State Chemistry **43**, 1 (2015).
[7] S. Vasala, J.-G. Cheng, H. Yamauchi, J. B. Goodenough, and M. Karppinen, Chemistry of Materials **24**, 2764 (2012).
[8] S. Vasala, H. Saadaoui, E. Morenzoni, O. Chmaissem, T.-S. Chan, J.-M. Chen, Y.-Y. Hsu, H. Yamauchi, and M. Karppinen, Phys. Rev. B **89**, 134419 (2014).
[9] S. Vasala, M. Avdeev, S. Danilkin, O. Chmaissem, and M. Karppinen, J. Phys.: Condens. Matter **26**, 496001 (2014).
[10] J. D. Reger and A. P. Young, Phys. Rev. B **37**, 5978 (1988).
[11] J. Rodriguez-Carvajal, Physica B **192**, 55 (1993).
[12] R. I. Bewley, T. Guidi, and S. Bennington, Notiziario Neutroni e Luce di Sincrotrone **14**, 22 (2009).
[13] M. Russina and F. Mezei, Nucl. Instrum. Methods in Phys. Rese. Sect. A **604**, 624 (2009).
[14] M. Russina and F. Mezei, Journal of Physics: Conference Series **251**, 012079 (2010).
[15] M. Nakamura, R. Kajimoto, Y. Inamura, F. Mizuno, M. Fujita, T. Yokoo, and M. Arai, J. Phys. Soc. Japan **78**, 093002 (2009).
[16] O. Arnold *et al.*, Nucl. Instrum. Methods Phys. Res. Sect. A **764**, 156 (2014).
[17] C. G. Windsor, *Pulsed Neutron Scattering* (Taylor & Francis Ltd, London, 1981) The time independent background was subtracted using MantidPlot, using data between 15000 μs and 18000 μs on MERLIN and 92000 μs and 98000 μs on LET.
[18] These were performed on a 7.85 g cylindrical vanadium (99.8 % purity) reference sample.
[19] R. I. Bewley, J. W. Taylor, and S. M. Bennington, Nucl. Instrum. Methods Phys. Res. Sect. A **637**, 128 (2011).
[20] H.-J. Koo and M.-H. Whangbo, Inorganic Chemistry **47**, 128 (2008).
[21] H.-J. Koo and M.-H. Whangbo, Inorganic Chemistry **47**, 4779 (2008).
[22] Http://elk.sourceforge.net.
[23] J. P. Perdew, K. Burke, and M. Ernzerhof, Phys. Rev. Lett. **77**, 3865 (1996).
[24] V. I. Anisimov, J. Zaanen, and O. K. Andersen, Phys. Rev. B **44**, 943 (1991).
[25] M. T. Czyżyk and G. A. Sawatzky, Phys. Rev. B **49**, 14211 (1994).
[26] A. I. Liechtenstein, V. I. Anisimov, and J. Zaanen, Phys. Rev. B **52**, R5467 (1995).
[27] S. Lebernegg, A. A. Tsirlin, O. Janson, and H. Rosner, Phys. Rev. B **89**, 165127 (2014).
[28] T. L. Chou, O. Mustonen, T. S. Tripathi, and M. Karppinen, J. Phys.: Condens. Matter **28**, 035802 (2016).
[29] J. P. Carlo, J. P. Clancy, T. Aharen, Z. Yamani, J. P. C. Ruff, J. J. Wagman, G. J. Van Gastel, H. M. L. Noad, G. E. Granroth, J. E. Greedan, H. A. Dabkowska, and B. D. Gaulin, Phys. Rev. B **84**, 100404(R) (2011).
[30] S. Toth and B. Lake, J. Phys.: Condens. Matter **27**, 166002 (2015).
[31] T. Moriya and K. Yosida, Prog. Theor. Phys. **9**, 663 (1953).
[32] J. Liu, H.-J. Koo, H. Xiang, R. K. Kremer, and M.-H. Whangbo, J. Chem. Phys. **141**, 124113 (2014).
[33] T. Koga, N. Kurita, and H. Tanaka, J. Phys. Soc. Jpn **83**, 115001 (2014).
[34] P. Babkevich, V. M. Katukuri, B. Fåk, S. Rols, T. Fennell, D. Pajić, H. Tanaka, T. Pardini, R. R. P. Singh, A. Mitrushchenkov, O. V. Yazyev, and H. M. Rønnow, arXiv:1605.09714.
[35] A. A. Aczel, P. J. Baker, D. E. Bugaris, J. Yeon, H.-C. zur Loye, T. Guidi, and D. T. Adroja, Phys. Rev. Lett. **112**, 117603 (2014).
[36] J. P. Carlo, J. P. Clancy, K. Fritsch, C. A. Marjerrison, G. E. Granroth, J. E. Greedan, H. A. Dabkowska, and B. D. Gaulin, Phys. Rev. B **88**, 024418 (2013).
[37] D. T. Adroja *et al.*, Unpublished.
[38] K. W. Plumb, A. T. Savici, G. E. Granroth, F. C. Chou, and Y.-J. Kim, Phys. Rev. B **89**, 180410 (2014).
[39] N. Tsyrulin, F. Xiao, A. Schneidewind, P. Link, H. M. Rønnow, J. Gavilano, C. P. Landee, M. M. Turnbull, and M. Kenzelmann, Phys. Rev. B **81**, 134409 (2010).
[40] N. B. Christensen, H. M. Rønnow, D. F. McMorrow, A. Harrison, T. G. Perring, M. Enderle, R. Coldea, L. P. Regnault, and G. Aeppli, Proc. Natl Acad. Sci. **104**, 15264 (2007).
[41] B. D. Piazza, M. Mourigal, N. B. Christensen, G. J. Nilsen, P. Tregenna-Piggott, T. G. Perring, M. Enderle, D. F. McMorrow, D. A. Ivanov, and H. M. Rønnow, Nature Phys. **11**, 62 (2015).
[42] C.-M. Ho, V. N. Muthukumar, M. Ogata, and P. W. Anderson, Phys. Rev. Lett. **86**, 1626 (2001).
[43] O. J. Burrows, G. J. Nilsen, E. Suard, M. Telling, and M. A. de Vries, arXiv:1602.04075.